Langmuir

Article

pubs.acs.org/Langmuir

Surface Pressure and Elasticity of Hydrophobin HFBII Layers on the Air−Water Interface: Rheology Versus Structure Detected by AFM Imaging

Rumyana D. Stanimirova,[†] Theodor D. Gurkov,[†] Peter A. Kralchevsky,[†,*] Konstantin T. Balashev,[‡] Simeon D. Stoyanov,[§,#] and Eddie G. Pelan[§]

[†]Department of Chemical Engineering, Faculty of Chemistry & Pharmacy, Sofia University, Sofia 1164, Bulgaria

[‡]Department of Physical Chemistry, Faculty of Chemistry & Pharmacy, Sofia University, Sofia 1164, Bulgaria

[§]Unilever Research & Development, 3133AT Vlaardingen, The Netherlands

[#]Laboratory of Physical Chemistry & Colloid Science, Wageningen University, 6703 HB Wageningen, The Netherlands

ABSTRACT: Here, we combine experiments with Langmuir trough and atomic force microscopy (AFM) to investigate the reasons for the special properties of layers from the protein HFBII hydrophobin spread on the air−water interface. The hydrophobin interfacial layers possess the highest surface dilatational and shear elastic moduli among all investigated proteins. The AFM images show that the spread HFBII layers are rather inhomogeneous, (i.e., they contain voids, monolayer and multilayer domains). A continuous compression of the layer leads to filling the voids and transformation of a part of the monolayer into a trilayer. The trilayer appears in the form of large surface domains, which can be formed by folding and subduction of parts from the initial monolayer. The trilayer appears also in the form of numerous submicrometer spots, which can be obtained by forcing protein molecules out of the monolayer and their self-assembly into adjacent pimples. Such structures are formed because not only the hydrophobic parts, but also the hydrophilic parts of the HFBII molecules can adhere to each other in the water medium. If a hydrophobin layer is subjected to oscillations, its elasticity considerably increases, up to 500 mN/m, which can be explained with compaction. The relaxation of the layer's tension after expansion or compression follows the same relatively simple law, which refers to two-dimensional diffusion of protein aggregates within the layer. The characteristic diffusion time after compression is longer than after expansion, which can be explained with the impedence of diffusion in the more compact interfacial layer. The results shed light on the relation between the mesoscopic structure of hydrophobin interfacial layers and their unique mechanical properties that find applications for the production of foams and emulsions of extraordinary stability; for the immobilization of functional molecules at surfaces, and as coating agents for surface modification.

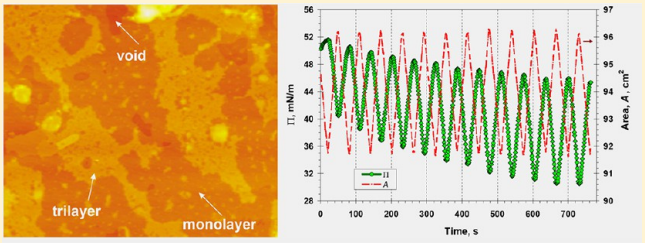

1. INTRODUCTION

The hydrophobins are fungal proteins that have attracted the attention of the scientific community with their strongly amphiphilic nature and ability to associate at interfaces. These features are promising in view of the use of hydrophobins for the stabilization of foams[1−5] and emulsions.[6−8] The properties of different types of hydrophobins have been reviewed,[9,10] and the perspectives for various scientific and practical applications have been noted.[11,12]

In this study, we are using the class II hydrophobin HFBII. It represents a small globular molecule, with dimensions of 24 × 27 × 30 Å and a structure that is described in detail in ref 13. An important feature of this molecule is the presence of a hydrophobic patch which is essentially flat,[13] while the remaining part of the protein is more hydrophilic. It should be noted that the "hydrophilic" part of HFBII includes several amino acids with hydrophobic side chains, which leads to attraction between the hydrophilic moieties of these proteins in the water medium and to the spontaneous formation of hydrophobin bilayers as a final stage of the thinning of foam films.[14] In other words, the HFBII molecule consists of a strongly hydrophobic part and a less hydrophobic (rather than really hydrophilic) part. The whole molecular structure is kept rigid by 4 disulfide bonds.

In the bulk of aqueous solutions, the hydrophobin molecules form dimers, tetramers, and larger aggregates.[13] The amphiphilic and "sticky" nature of these molecules is responsible for their adsorption and aggregation at air−water and oil−water interfaces. A prominent characteristic of the surface layers is the strong association of the molecules in the lateral direction,[15] which leads to solidification of such adsorption layers. This phenomenon has been established by both observations with atomic force microscopy (AFM)[16−18] and by surface rheological studies.[1,3,19,20]

Received: February 6, 2013
Revised: April 23, 2013
Published: April 23, 2013

   dx.doi.org/10.1021/la4005104 | *Langmuir* 2013, 29, 6053−6067

AFM pictures at nanometer resolution provide useful information about the morphology of layers that consist of class II hydrophobins HFBI and HFBII.[16−18] Their molecules are closely packed to form regions of condensed phase, but voids are also present in the interfacial layers. In other words, the whole mesoscopic structure is not entirely compact. The cross bonding of the class II hydrophobins has been shown to be a rapid process (taking milliseconds), which happens without any conformational changes in the individual molecules.[9]

On the surfaces of bubbles and drops, the HFBII forms solid-like stiff layers resembling skin.[1,19] Because the protein layer at the bubble surface solidifies during the process of stirring, the bubbles preserve their instantaneous nonspherical shape after ceasing the agitation.[19] The rigidity of the hydrophobin adsorption layers at the air−water interface is manifested also by the appearance of periodic wrinkles (ripples) upon compression.[17,19,21] High values of the surface shear elasticity, which makes the difference between solid and fluid interfacial layers, have been measured with hydrophobin layers.[1,3] For example, Cox et al.[1] found that upon shear oscillations (of frequency 1 Hz, and a very small amplitude, 5 mrad), the elasticity modulus can exceed 500 mN/m. By measurements in different kinetic regimes, it was established that the sheared hydrophobin layers exhibit a viscoelastic behavior, which obeys the combined Maxwell−Herschel−Bulkley law.[22,23] After ceasing the shearing, the layers solidify in such a way that the stress relaxes following a modified Andrade cubic-root law.[22]

The dilatational elasticity is also quite high. Alexandrov et al.[20] investigated fluid layers (at low HFBII concentrations) with the pendant drop method (using drop shape analysis, DSA), as well as with spread layers in a Langmuir trough. In both cases, the dilatational elastic modulus reached 150−200 mN/m. The HFBII layers were found to exhibit purely elastic behavior upon expansion and compression (i.e., no effects from surface dilatational viscosity have been detected). Blijdenstein et al.[3] applied large continuous deformations in a Langmuir trough and measured dilatational elasticities of 300−350 mN/m for spread HFBII layers.

Our goal in the present study is to investigate the reason for the high elasticity of the hydrophobin interfacial layers in relation to their mesoscopic structure. For this goal, the Langmuir trough and AFM measurements have been combined. HFBII layers have been spread in a Langmuir trough on the air−water interface and subjected to compression, which leads to an increase of the layer's surface pressure (Π). At a given Π, samples from the interface are taken for AFM imaging. Moreover, at a given Π, oscillations of the layer's area are imposed (by varying the distance between the barriers in the trough), and the surface elasticity (E) is determined. This approach allows us to relate the measured Π and E to the layer's structure observed by AFM.

In the next section, the materials and methods used are described. The results are presented in three sections reflecting three different kinetic regimes: (i) compression at a fixed rate (Surface Morphology Versus Surface Pressure), (ii) interfacial oscillations (Dilatational Elasticity by Area Oscillations), and (iii) relaxation after a fast compression or expansion (Relaxation Kinetics after Expansion or Compression). The kinetic regime of relaxation (diffusion, barrier, or mixed control) is identified and discussed in view of the data for the mesoscopic structure of the hydrophobin layers obtained by the AFM imaging.

2. MATERIALS AND METHODS

2.1. Materials. In our experiments we used the protein HFBII, which is a class II hydrophobin isolated from the fungus *Trichoderma reesei*. The procedure for its production and purification is described in ref 19. We used a sample of HFBII supplied by Unilever R&D (Colworth, U.K.), in the form of a dry powder. Stock solution of 0.34 wt % was prepared with deionized water from a Milli-Q Organex purification system (Millipore, USA). The natural pH of the solution was 5.6. In some experiments, we worked at pH = 8.5, which was adjusted by the addition of small portions (200 μL) of 10^{-3} M NaOH.

The stock solution looked turbid because of the existence of relatively large HFBII aggregates in the bulk. To ensure reproducibility of the experiments, the solution was sonicated in an ultrasound bath for 5 min just before its use. The intensity of the ultrasound was low enough to disperse the hydrophobin aggregates without causing any sonochemical effects, like changes in the protein secondary structure. The sonication makes the HFBII solution completely clear and transparent. After that, the growth of aggregates begins again and the solution becomes gradually turbid within about 10 min. The stock solution was stored in a freezer at −18 °C. Before sonication and use, it was kept for some time at room temperature to warm up. All experiments were carried out at 23 °C.

2.2. Langmuir Trough Method. This method is a convenient tool for investigating the surface rheology and chemical reactions with protein films on liquid interfaces.[24−27] In our experiments, the two-dimensional rheology of HFBII layers spread on the air−water interface was studied by a Langmuir trough with a traditional design. The model of the used apparatus was 302 LL/D1, manufactured by Nima Technology Ltd. The dimensions of the trough were 10 × 20 cm. The interfacial area was varied by two parallel Teflon barriers, which moved symmetrically. Their speed of linear translation was constant and was set by the software. The surface tension (σ) was measured with a Wilhelmy plate made of chromatographic paper. The paper plate prevented contamination by impurities (new piece was used in each experiment) and also ensured complete wetting. To prevent evaporation effects, the Langmuir trough is closed under a transparent cover together with an open vessel with water that ensures vapor saturation.

Because the imposed deformation is unidirectional, the stresses engendered in the elastic (solidified) adsorption layer are anisotropic. Such a layer possesses both shear and dilatational elasticity,[3,20,22,23] characterized by the dilatational (K) and shear (μ) moduli. In principle, it is possible to determine both K and μ by placing the Wilhelmy plate parallel and perpendicular to the barriers in the Langmuir trough.[28] For our goals, it was sufficient to measure only the sum, $E = K + \mu$, by positioning the Wilhelmy plate in the middle between the two barriers, parallel to them. The parameter $E = K + \mu$ has the meaning of total elasticity, which is used here as a dynamic characteristic of the interfacial layer in relation to its mesoscopic structure at various degrees of compression. Detailed experimental studies on the dilatational[20] and shear[22,23] elasticity of HFBII layers have been recently published.

Data acquisition is performed continuously (every one second). The apparatus records the area between the barriers (A) and the surface pressure (Π), as functions of time (t). By

dx.doi.org/10.1021/la4005104 | Langmuir 2013, 29, 6053−6067

definition, Π is the decrease of the surface tension caused by the presence of amphiphilic species, $\Pi = \sigma_0 - \sigma$, where σ_0 refers to the bare air−water interface. At 23 °C, σ_0 = 72.3 mN/m.

In a typical experiment, the trough vessel is first filled with clean water (Millipore grade). The Wilhelmy plate is placed in working position. The barriers are adjusted to enclose an area of 120 cm^2. Then, drops of aqueous HFBII solution (0.34 wt %) are gently put on the aqueous surface, at different places that are roughly equally far from the Wilhelmy plate, the barriers, and the trough walls. The total amount of the protein solution is usually 32.9 μL, distributed as 5−6 aliquots with a micropipet. Then, the layer is left at rest for about 15 min to equilibrate. Next, the layer is compressed by the barriers, and the measurements proceed according to the chosen protocol. We applied (i) a continuous large compression and (ii) compression−expansion cycles of small amplitude, the relative area change being at most ±2.4%. The barrier speed is selected to be such that dA/dt = 4, 5, 10, or 20 cm^2/min in different runs.

To know the spread amount of protein, we have to dissolve the HFBII into an organic solvent that is immiscible with water, like chloroform. However, the organic solvent could denature the hydrophobin. For this reason, as described above, HFBII is deposited as water drops, and consequently, a certain fraction of the protein goes into the bulk during the drop coalescence with the water subphase. Hence, we do not know the exact spread amount of HFBII. We prefer this situation to denaturing the protein. We measured (i) Π versus the total area A, (ii) Π versus time (relaxations, oscillations), and (iii) AFM images versus Π. As demonstrated below, the analysis of the obtained data yields rich information about the properties and behavior of the HFBII layers subjected to deformations.

2.3. AFM Sample Preparation. We deposited the HFBII layers with their hydrophobic side on a hydrophobic solid substrate. For this goal, a hydrophobized mica plate was pressed against the HFBII laden air−water interface from above. This corresponds to the Langmuir−Schaefer (LS) method, described by Houmadi et al.[29] The barriers in the Langmuir trough have been used for compression of the HFBII layer until a given surface pressure Π is reached. In different runs, samples have been taken at Π = 25, 35, 48, and 62 mN/m (see below).

Freshly cleaved mica plates of dimensions about 1 × 1 cm were used. The active surface of the plates was kept for a few hours in vapors of hexamethyl disilazane (HMDS), a hydrophobizing agent. The mica leaf was attached to a homemade holder on the dipper mechanism of the Langmuir trough. After preparation of the air−water interface, dry mica is set to touch it from above. Starting from a height of 1−2 cm in the air phase, the dipper gradually lowers the level of the horizontal mica plate until it touches the surface. The plate stays fixed in this position for a few minutes to ensure firm adhesion of the layer to the hydrophobized mica surface. Afterward, the plate is raised up at a given low speed, until it fully detaches from the interface. Simultaneously, the trough area is being contracted with the two barriers to hold the surface tension almost constant and prevent detachment and damaging of the deposited layer. Finally, the plate with the adherent protein layer is dried in an air environment.

We tried also Langmuir−Blodgett (LB) transfer with a hydrophilic plate initially immersed in the aqueous phase. In these experiments, the deposited layer was broken to pieces, or there was no deposited layer at all. The most probable reason is that the HFBII (multi)layer subjected to compression is highly elastic, and it breaks when the LB plate is pulled out of the water phase. Perhaps, the adhesion of the layer to the hydrophilic substrate (in water) is too weak. The LS transfer, on the other hand, gives good results; the hydrophobized mica is uniformly covered with an unbroken layer. This could be due to much stronger adhesion of the HFBII layer to the hydrophobic support (in air). For this reason, only LS transfer has been used further on.

The HFBII is a rigid shape-persistent protein molecule; it is not expected to undergo essential conformational changes at the air−water interface and when dried on a solid surface.[13,16−18] In particular, the thickness of a dried HFBII monolayer registered by AFM is ≈3 nm (see below), which coincides with the size of the HFBII molecule determined by X-ray structural analysis of crystals.[13] Hydrophobins are very hard to denature; their aqueous solutions have been heated to 90 °C without any sign of protein denaturing.[16,30] There may be some minor changes in shape for hydrophobins when they self-assemble, but this is a part of their function and should not be confused with denaturing.[16]

What concerns the mesoscopic structure of the protein interfacial layer, we suppose, is that its topography is not essentially influenced by its LS deposition on the smooth surface of the mica sheet. In other words, we assume that the AFM images reflect almost the same structure as that of the layer at the air−water interface.

2.4. AFM Method and Equipment. AFM imaging was performed on the NanoScope Multi Mode V system (Bruker Inc., Germany), operating in the tapping mode in air at room temperature. The setup uses a stationary probe, which in tapping mode is excited by a piezoelectric stack to oscillate up and down while the substrate is scanned by moving it beneath the probe. The mica supported sample is fixed on a round metal disk ("puck"), which is magnetically attached to the top of the scanner tube. This tube translates the sample back and forth horizontally, while the probe extracts information from the deflection of the cantilever as the tip encounters the surface. The return signal reveals information about the vertical height of the sample surface and some other features of the material deposited on mica. We used silicon cantilevers (Tap 300 Al-G, Budget Sensors, Innovative Solutions Ltd., Bulgaria) with 30 nm thick aluminum reflex coating. In accordance with the producer's datasheet, the cantilever spring constant was in the range of 1.5−15 N/m, and the resonance frequency was 150 ± 75 kHz. The tip radius was less than 10 nm. Before imaging, the samples were thoroughly dried with N_2 gas. The scan rate was set at 1 Hz, and the images were captured in the height and phase modes with 512 × 512 pixels in a JPEG format. Subsequently, all images were flattened using Nanoscope (version 7.30). The samples were typically scanned in several different locations along the mica leaf. The obtained AFM images are presented and discussed in AFM Images of Spread HFBII Layers.

2.5. Ellipsometry. The ellipsometric measurements of protein adsorption were carried out with a smaller trough of a different aspect ratio, installed in the ellipsometer. To obtain similar surface coverage as in the Langmuir trough (Langmuir Trough Method), we placed 38 μL from a 0.15 wt % HFBII solution on an air−water interface of area 77.4 cm^2. This amount would give a 7.4 mg/m^2 protein surface coverage. The water subphase contains 10 mM NaCl.

We used the "rotating analyzer" apparatus, described in detail elsewhere.[31,32] The setup allows measuring the ellipsometric

dx.doi.org/10.1021/la4005104 | Langmuir 2013, 29, 6053−6067

signal in intervals of one second; thus, the time-dependence of the layer properties is examined. In the reflected laser light, only the phase difference between the two perpendicular directions of polarization is useful and measurable when the interfacial layer of deposited material is very thin.[32] Then, the ellipsometric angle Δ carries the meaningful information, and in this case, the surface coverage per unit area (Γ) is proportional to the change of Δ (with respect to the bare surface, Δ_0). We apply the relation Γ (mg/m^2) $\approx 0.6\ (\Delta-\Delta_0)$ for proteins.[32]

The ellipsometric measurements have been carried out to confirm whether we are dealing with protein monolayer or multilayer. Because the ellipsometer spot diameter is ≈1 mm, it gives only averaged values of the protein adsorption, Γ. Much more detailed information on the interfacial layer structure is provided by the AFM, which shows the surface topography on the micrometer scale.

3. SURFACE MORPHOLOGY VERSUS SURFACE PRESSURE

Here, we present results for the surface pressure (Π) versus the surface area (A) obtained by compression of hydrophobin interfacial layers in a Langmuir trough. At different Π values, samples from the protein layer have been taken and investigated by AFM to see what the interfacial mesoscopic structure is at the different stages of compression.

3.1. Surface Pressure Isotherms. Figure 1 (panels a and b) show data for the surface pressure of the HFBII layer spread on the surface of pure water in the Langmuir trough (drops of total volume 32.9 μL from 0.34 wt % HFBII solution placed on the air−water interface). The upper curve in Figure 1a corresponds to a continuous compression of the spread layer at a constant speed = 10 cm^2/min. As seen in the figure, in this run, Π increases with an almost constant slope, and afterward, at Π > 65 mN/m, it exhibits a tendency to level off. The decrease of the slope is accompanied by the appearance of periodic ripples in the spread layer, which are visible by Brewster angle microscopy. With hydrophobin layers, such ripples (wrinkles) have been experimentally observed[19] and theoretically investigated.[21] The regular sinusoidal ripples appear in interfacial layers of high bending elastic modulus (k_c), which opposes the surface wrinkling. One should note the difference between the sinusoidal ripples and the conventional collapse that appears as large folds in soft interfacial layers (with negligible k_c effect) or in any flexible layers at sufficiently large deformations; for details, see ref 21.

In Figure 1a, the lower discontinuous $\Pi(A)$ isotherm, which is composed of five stages, has been obtained in the following way. After each of the stages 1−4, the compression of the spread layer stops and area oscillations of (relatively small) amplitude, $\Delta A \approx \pm 2.4$ cm^2, have been imposed for a period of 12−13 min. After the end of the oscillations, Π is lower than before their beginning, typically, with 10 mN/m and more. The next compression stage begins from this lower value of Π. At the last stage 5, the surface pressure levels off, which is accompanied by the appearance of periodic wrinkles (ripples) in the spread layer. As mentioned above, the wrinkling of compressed hydrophobin layers has been observed and analyzed in several studies.[1,17,19,21]

The surface elasticity, E, is defined in the standard way:

$$E = -\frac{d\Pi}{d \ln A} \qquad (1)$$

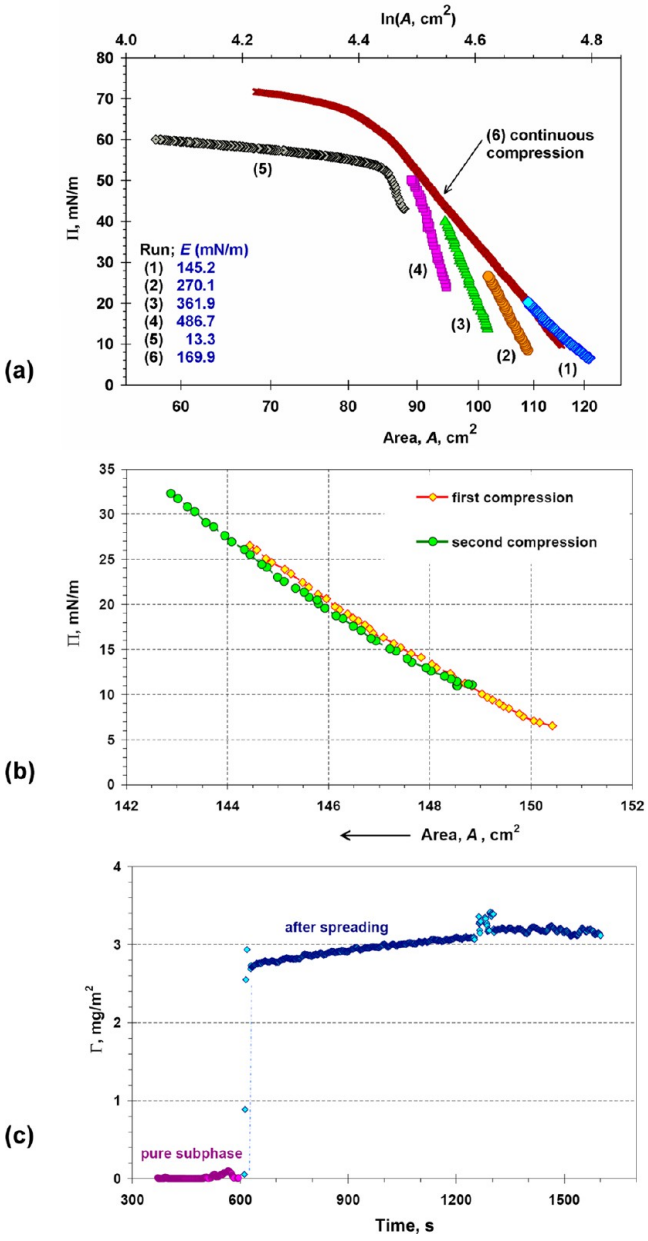

Figure 1. (a) Surface pressure (Π) vs A (in log scale) for HFBII layers spread in a Langmuir trough and subjected to stepwise (1−5) and continuous (6) compression. (b) Π vs A for two consecutive compressions of the same HFBII layer at speed 20 cm^2/min. (c) Ellipsometric measurement of the surface concentration (Γ) vs time: spreading of 38 μL from 0.15 wt % HFBII solution on the air−water interface.

The above equation defines E as a macroscopic phenomenological parameter: both Π and A can be directly measured and substituted in eq 1 to calculate the elasticity. A is the projected geometrical area. The real interface can be microscopically undulated or may have a nonuniform thickness (e.g., regions of monolayer, multilayers, and voids). The dependence of E on the degree of compression/extension can be interpreted in terms of the mesoscopic structure of the interfacial layer. For example, two regimes of dilatation are observed with phospholipid bilayers: (i) soft exponential relation between tension and area due to the presence of short-wavelength

dx.doi.org/10.1021/la4005104 | Langmuir 2013, 29, 6053−6067

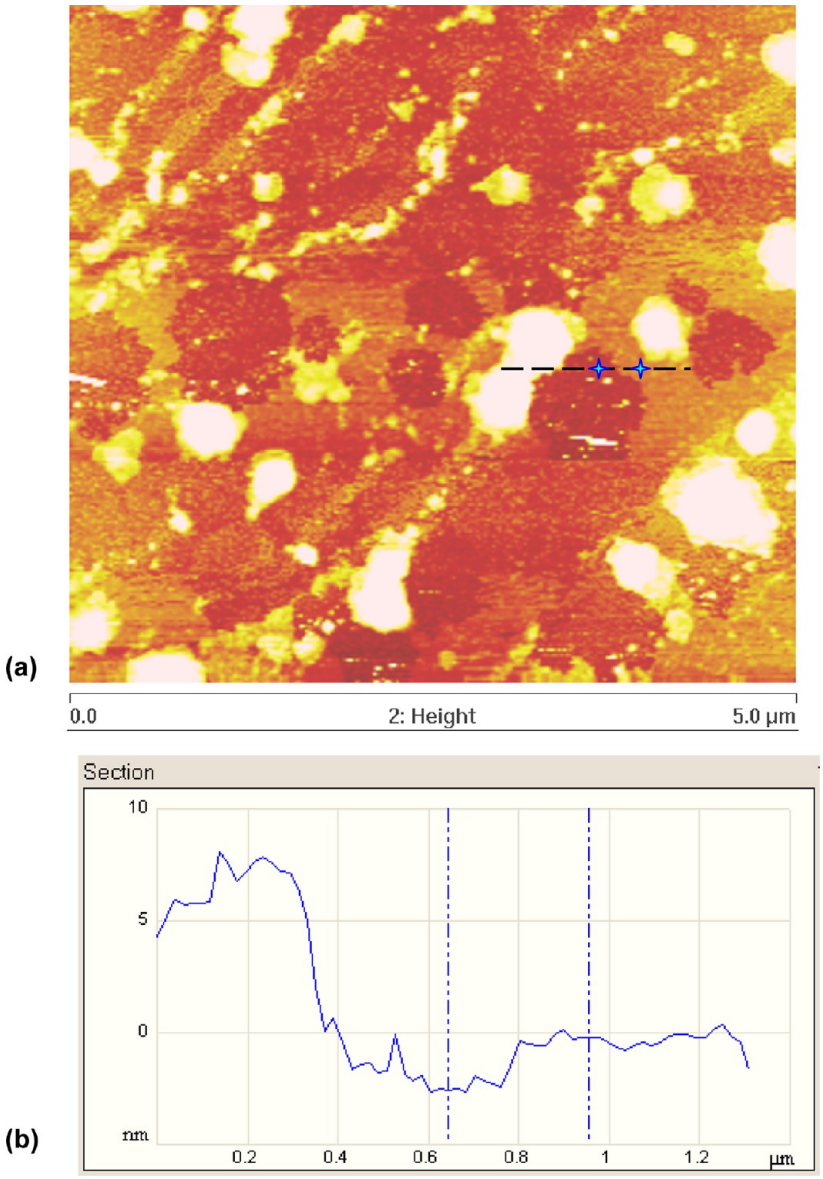

Figure 2. (a) AFM image of a HFBII layer at Π = 25 mN/m; the layer has been initially spread and then compressed from 125 to 99.8 cm^2 at a speed of 4 cm^2/min. (b) Thickness of the HFBII layer vs the distance along the section (the dashed line) in Figure 2a. The height difference (Δh) between each of the two points is independent of the position of the zero on the vertical axis, which is arbitrarily chosen.

undulations, followed by a crossover to (ii) stiff linear proportionality (direct expansion) up to the rupture point.[33,34]

In the case of continuous compression (the upper curve in Figure 1a), the wide region of constant slope, 87 ≤ A ≤ 115 cm^2 (stage 6), corresponds to a constant elasticity, E = 169.9 mN/m, which is close to that of stage 1 of the discontinuous isotherm, E = 145.2 mN/m. For stages 2, 3, and 4 of the discontinuous isotherm, the slopes (and the respective E values) significantly increase, up to E = 486.7 mN/m for stage 4 (Figure 1a). This rise of E can be explained with a compaction of the protein layer during the preceding area oscillations. The respective structural changes in the layer are seen in the AFM images (AFM Images of Spread HFBII Layers).

The wrinkling of the layer during stage 5 at Π ≥ 52 mN/m (Figure 1a) corresponds to an effective low elasticity, E = 13.3 mN/m, which is markedly lower than the E values for the preceding stages. Note that the periodic wrinkles (ripples) appear at $\sigma \approx 0$ because a positive surface tension (σ) strongly suppresses the wrinkling.[21] Because the HFBII layer solidifies at Π ≥ 22 mN/m,[20] σ is not constant throughout the layer. The wrinkling begins locally in separate interfacial zones, as seen by the microscopic observations. In view of the theoretical predictions,[21] we can suppose that these are the zones where locally, $\sigma = 0$. (Here, the scalar σ is the thermodynamic surface tension; see eq 3.21 in ref 21.) The measurement gives Π = 55−60 (instead of 72) mN/m for stage 5 (i.e., the protein layer is locally extended in the vicinity of the Wilhelmy plate), which leads to $\sigma_{xx} > 0$ in that vicinity. (σ_{xx} is the component of the surface stress tensor, which is measured by the Wilhelmy plate.)

Numerous studies with molecular films spread on water[35−39] indicate that the collapse begins at a surface pressure, $\Pi = \sigma_0 - \sigma$, that is markedly lower than 72 mN/m. This seems to contradict the theoretical prediction[21,40] that the membrane wrinkling happens at $\sigma \approx 0$. As already mentioned, a possible explanation of this paradox could be given if we take into account the fact that the measuring procedure includes the

dx.doi.org/10.1021/la4005104 | Langmuir 2013, 29, 6053−6067

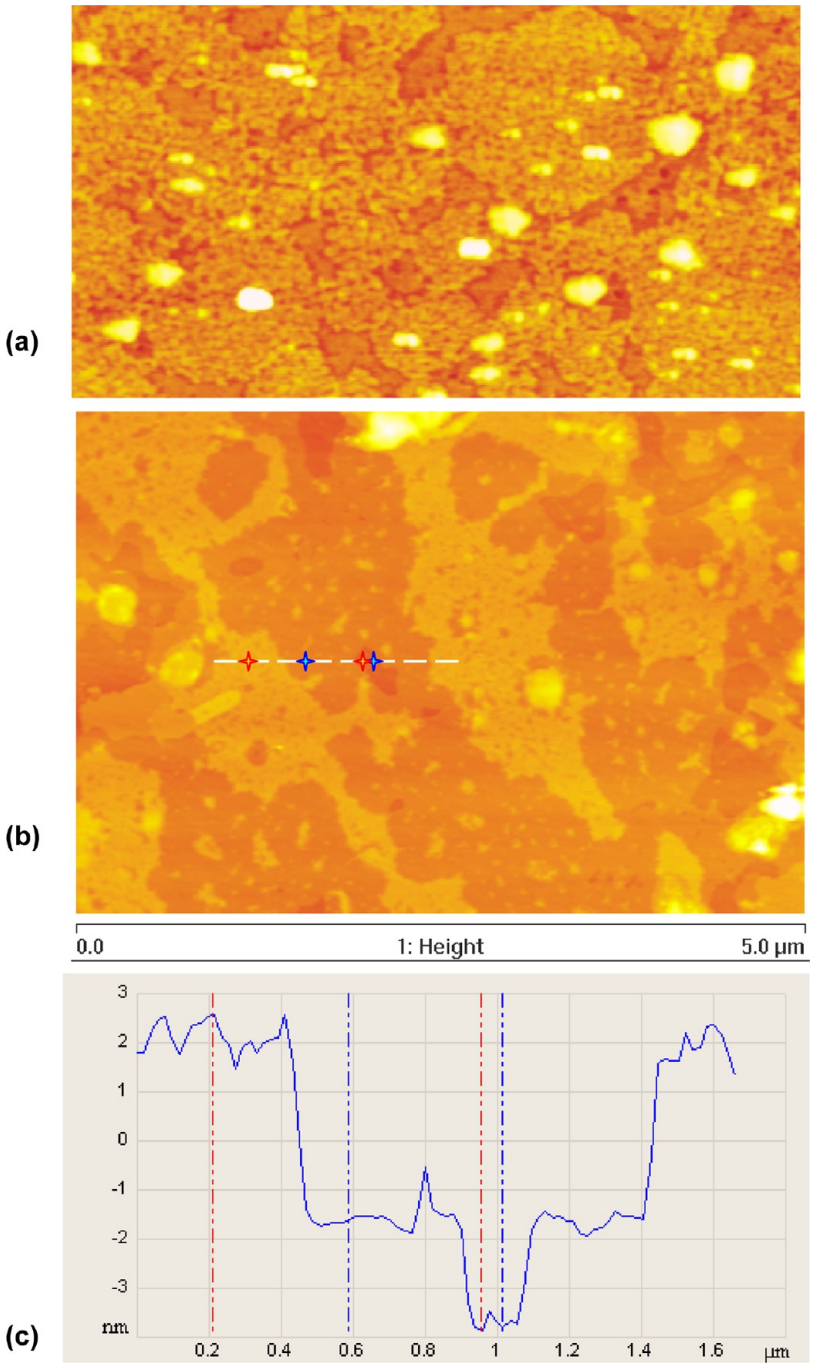

Figure 3. AFM images of a spread HFBII layer at two different surface pressures: (a) Π = 35 mN/m, length of the picture = 2 μm, and (b) Π = 48 mN/m, length of the picture = 5 μm. (c) Thickness of the HFBII layer vs the distance along the section (the dashed line) in Figure 3b. The position of the zero on the vertical axis is arbitrarily chosen; Δh = 2.2 and 6.4 nm for the lower and upper steps with respect to the bare mica surface.

formation of a curved and pulled up meniscus around the Wilhelmy plate. This creates a local extension in the elastic membrane around the plate, which in turns gives rise to a positive local σ that is detected by the balance.[21] Despite the fact that the Wilhelmy plate measures the local σ in the zone of its contact with the interfacial membrane, the differentiation of the obtained Π to get E (see eq 1) and the relaxation of Π with time (Relaxation Kinetics After Expansion or Compression) bring valuable information for the rheological response of the interfacial layer to deformations. It should be noted that all rheometers for measurements with viscoelastic bodies register the stress acting on the measuring tool, but they do not give any direct information for the distribution of stresses in the interior of the investigated material. (The full stress distribution can be evaluated in the frame of an appropriate rheological model.)

In Figure 1b, we check whether the spread HFBII molecules can desorb into the subphase of pure water. For this reason, a diluted adsorption layer was formed by dropping 32.9 μL of the 0.34 wt % HFBII solution, the same amount as in Figure 1a but on a greater surface area of 150 cm^2 (instead of 120 cm^2 in Figure 1a). After the spreading, we waited for 35 min before the start of the first compression. During this period, equilibration of the protein layer is expected, including release of

dx.doi.org/10.1021/la4005104 | *Langmuir* 2013, 29, 6053−6067

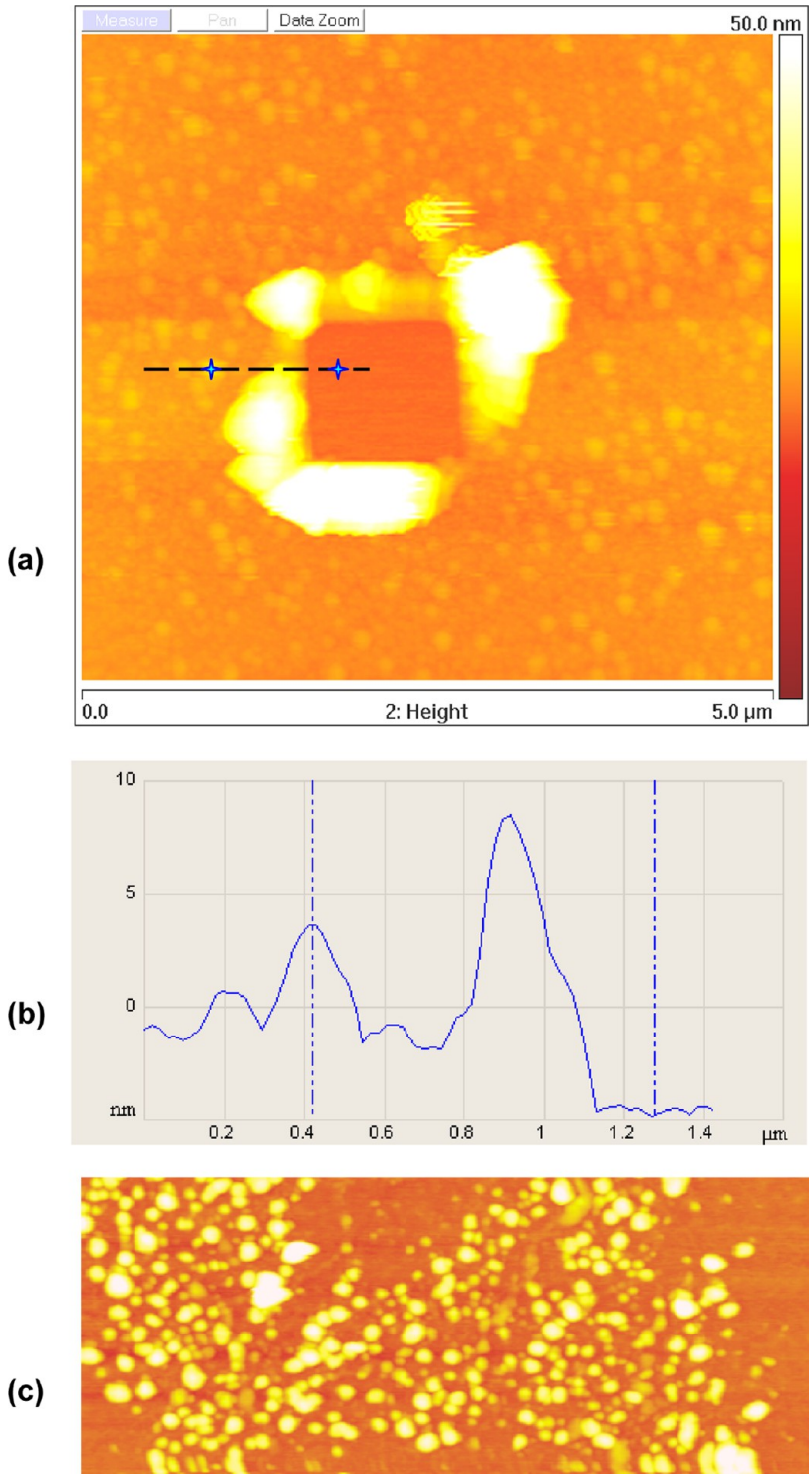

Figure 4. (a) AFM image of a spread HFBII layer at Π = 62 mN/m; material has been scratched out at the center, so that a square spot of bare mica is created. (b) Thickness of the HFBII layer vs the distance along the section (the dashed line) in Figure 4a; the thickness difference between two positions denoted by vertical lines is Δh = 8.4 nm. (c) AFM image at Π = 62 mN/m for a layer spread on the surface of a 10 mM NaCl solution; length of the picture = 2 μm.

hydrophobin molecules from adsorbed aggregates that have been formed during the few minutes between the solution's sonication and deposition at the air−water interface. After the first compression, the interfacial film was kept at rest for 15 min. Next, the layer was expanded to a 149 cm^2 surface area. We waited again for 15 min for equilibration and carried out the second compression. Both compressions were relatively small (ΔA < 8 cm^2, $\Pi \leq$ 33 mN/m) and were carried out at a speed of 20 cm^2/min. The two experimental curves in Figure 1b are practically coinciding, which confirms the irreversibility of HFBII adsorption at the air−water interface previously established.[20] In the last study, automatic axisymmetric shape analysis was applied to buoyant bubbles attached to the tip of a capillary. HFBII adsorbed on the bubble surface from an

dx.doi.org/10.1021/la4005104 | *Langmuir* 2013, 29, 6053−6067

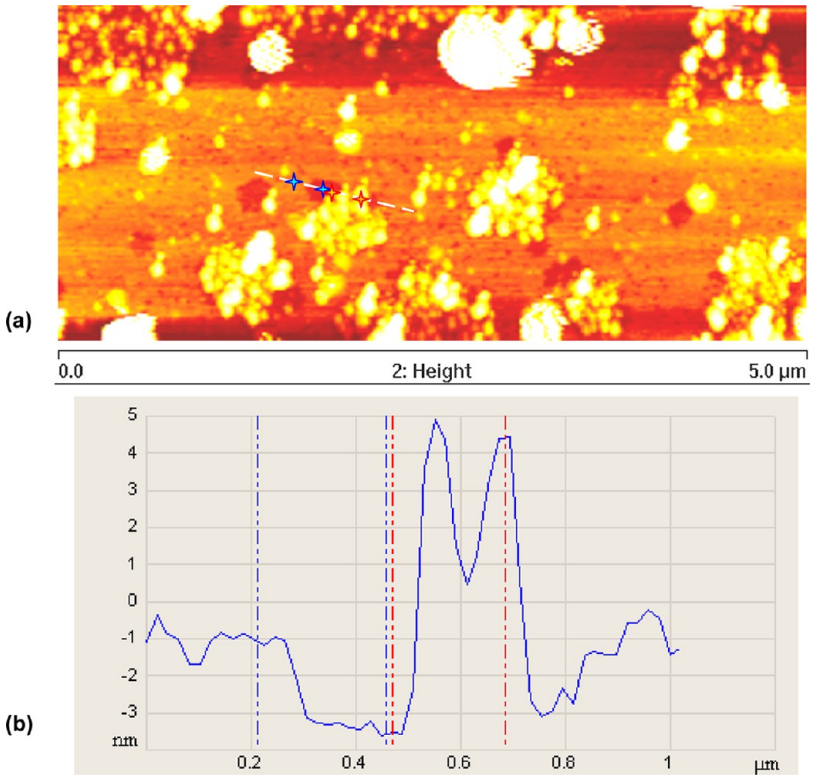

Figure 5. (a) AFM image of a HFBII layer which has undergone, first, compression to Π = 50 mN/m and after that oscillations for 13 min at a speed 10 cm^2/min. (b) Thickness of the HFBII layer vs the distance along the section (the dashed line) in Figure 5a. The thickness difference between the lowest point and two "uplands" denoted by vertical lines is Δh = 2.6 and 7.9 nm.

aqueous hydrophobin solution, which was next exchanged with pure water. The measured surface pressure, storage, and loss dilatational moduli remained the same. Hence, having once adsorbed at the air−water interface, HFBII does not desorb even in pure water.[20]

The comparison of panels a and b of Figure 1 shows that Π = 30 mN/m is reached at A = 103.5 and 143.4 cm^2, respectively. This difference can be explained with the release of hydrophobin molecules from adsorbed aggregates during the longer waiting period (35 vs 20 min), corresponding to the experiment described in Figure 2b.

3.2. Ellipsometric Study of the Surface Coverage. The process of spreading is very fast (Figure 1c). The adsorption Γ spontaneously reaches a relatively stable value which further changes only slightly and slowly, as some material is distributed more evenly over the interface. The equilibrium Γ is in the range of 2.9−3.1 mg/m^2, or 0.40−0.43 × 10^{-10} mol/cm^2, the molecular mass of HFBII being 7200 g/mol.

The obtained Γ can be compared with values reported by Zhang et al.,[41] who measured Γ after adsorption from the bulk of HFBII solutions at 0.002−0.2 g/L concentrations. They found Γ to be approximately constant and equal to 2.82 mg/m^2, or 0.39 × 10^{-10} mol/cm^2, which practically coincides with our results in Figure 1c. It turns out that the two quite different procedures (spreading vs adsorption) lead to almost the same protein surface density. However, this coincidence could be fortuitous because HFBII is liable to form multilayers and surface aggregates (see below).

Let us estimate the adsorption Γ from the molecular size, assuming that the interface is fully covered by a densely packed monolayer of HFBII. Taking a cross-section of 24 × 27 Å per molecule[13] at close packing, we calculate Γ = 1.84 mg/m^2. The real surface coverage should be somewhat lower because the monolayers contain voids.[16−18] However, our direct measurements, as well as those in ref 41, show that the experimental Γ is significantly greater than 1.84 mg/m^2, viz. 2.8−3.1 mg/m^2. This is strong evidence that the hydrophobin does not cover the air−water interface with a uniform monolayer. The presence of domains with greater thickness (e.g., zones with trilayer) is responsible for the accumulation of more material (AFM Images of Spread HFBII Layers).

3.3. AFM Images of Spread HFBII Layers. The protein layers considered here have been formed by spreading 32.9 µL of 0.34 wt % HFBII on the air−water interface in the Langmuir trough at an initial area of 125 cm^2 between the barriers (see Langmuir Trough Method). Next, the area A was decreased at a speed 4 cm^2/min to a certain value. After that, a sample of the layer was taken on a mica plate for AFM observations (see AFM Sample Preparation for details).

Figure 2a shows the AFM image of a hydrophobin layer with Π = 25 mN/m obtained by compression of the spread layer to A = 99.8 cm^2. In the image, the dark spots correspond to voids in the protein layer, which contain some small dispersed spots of pale color, probably HFBII aggregates. In addition, portions of the much thicker layer are seen in Figure 2a as bright spots. Most probably, they are hydrophobin aggregates, which have been present in the drop of relatively concentrated HFBII solution that has been deposited at the air−water interface in the Langmuir trough; see Surface Pressure Isotherms. The zones of intermediate color intensity represent a monolayer insofar as the height difference $\Delta h \approx$ 2.3 nm, relative to the voids, corresponds to one layer of HFBII molecules; see the cross section in Figure 2b. The bright spots have a greater thickness corresponding to 3−5 protein layers. Because the

dx.doi.org/10.1021/la4005104 | Langmuir 2013, 29, 6053−6067

scales along the horizontal and vertical axes in the AFM images are rather different, micrometers versus nanometers (cf. Figure 2b), the bright spots actually represent "uplands" with the shape of flat plateaus.

Despite the relatively low surface pressure, Π = 25 mN/m, the results in Figure 2 show that the surface is highly inhomogeneous. Its structure is completely dissimilar to a uniform monolayer. If the experimental surface pattern is considered as a two-dimensional dispersion, the voids are the disperse phase (they form separate spots), whereas the protein layer of nonuniform thickness is the continuous phase. This result is in agreement with the finding[20] that the HFBII adsorption layers solidify at $\Pi \approx 22$ mN/m. The solidification can be considered as a percolation threshold: for $\Pi < 22$ mN/m, the voids are the continuous phase, whereas at $\Pi > 22$ mN/m, the pieces of protein monolayer or multilayer touch each other and form a continuous elastic membrane that encloses dispersed voids.[20] This picture corresponds to the AFM micrograph in Figure 2a.

Figure 3a displays an AFM image taken at a higher surface pressure, Π = 35 mN/m. The protein layer resembles that in Figure 2a, but the dark spots (the voids) are markedly smaller. Large empty areas are missing at all. In other words, the area fraction of the voids is lower at Π = 35 mN/m. The bright spots in Figure 3a indicate the presence of thicker regions resembling isolated high plateaus.

Figure 3b shows the surface topography at Π = 48 mN/m. The area fraction of the voids (isolated dark spots) is relatively small. Some high plateaus are also present, similarly to the other cases discussed above. The most remarkable feature in Figure 3b is the coexistence of monolayer (darker zones) and trilayer (brighter zones) in large areas. One can determine the height steps, Δh, with respect to the bare mica. In Figure 3c, the lower steps of height $\Delta h \approx 2.2$ nm refer to a monolayer, whereas the "highlands" with $\Delta h \approx 6.4$ nm correspond to a trilayer.

Figure 4a shows an AFM image of a spread HFBII layer that has been compressed to Π = 62 mN/m. The numerous round spots represent protrusions (pimples). To determine the height of the protrusions, we used the clean mica surface as reference. By means of the AFM tip (in contact mode), some material was scratched out and the bare mica was exposed (see the square spot in Figure 4a). The height measurement (Figure 4b) reveals that the selected "grain" corresponds to $\Delta h \approx 8.4$ nm, which is slightly above a trilayer. Figure 4c also corresponds to Π = 62 mN/m, but this time the hydrophobin was spread on an aqueous subphase that contains 10 mM NaCl. In general, the surface topography is similar in Figure 4 (panels a and c). In the presence of NaCl, the protrusions are better pronounced.

Figure 5a is an AFM image of a hydrophobin layer after oscillations. Initially, HFBII was spread on the air–water interface and then compressed from 123 to 99.6 cm^2. Before the oscillations, the surface pressure was $\Pi \approx 50$ mN/m at A = 99.6 cm^2. After reaching that state, oscillations of relative amplitude $\Delta A/A \approx \pm 2.4\%$ have been applied for 13 min at a speed of 10 cm^2/min. Figure 5a indicates that the oscillations have led to the aggregation of the pimples (such as those in Figure 4) into larger clusters. The thickness measurements (Figure 5b) show that for the background layer and the hill, the thickness is Δh = 2.6 and 7.9 nm, respectively, so that they can be identified as a monolayer and a trilayer.

3.4. Discussion. The data in Figures 3–5 indicate the preferential formation of monolayers and trilayers of HFBII. Such a tendency was observed also with layers from the phospholipid 1,2-di-[*cis*-9-octadecenoyl]-*sn*-glycero-3-phosphocholine (DOPC).[42] Physically, the formation of multilayers composed of an odd number of layers at the air–water interface happens in the presence of tail–tail and head–head attraction of amphiphilic molecules. Thus, the uppermost hydrophobic layer faces the air, whereas the lowermost hydrophilic layer faces the water phase. The hydrophobic patches of the HFBII molecules are facing the air. As already mentioned, in water, not only the hydrophobic but also the hydrophilic parts of the HFBII molecules attract each other, which is manifested by the spontaneous formation of self-assembled HFBII bilayers (S-bilayers).[14,19] In the case of such amphiphilic molecules, the symmetric configuration of an air/water/air film favors the formation of bilayers (more generally, layers with even number of molecules), whereas the asymmetric air/water interface favors the formation of monolayers, trilayers, etc. (odd number of layers).

The AFM images show that two different patterns of trilayer are formed. First, the trilayer can appear in the form of large surface domains, as in Figure 3b. Second, the trilayer can appear in the form of numerous pimples of submicrometer diameter; see Figures 4 (panels a and c) and 5a. We could hypothesize that the two types of mesoscopic structures are created by two different mechanisms.

The trilayer domains (Figure 3b) could be formed by a process of folding and subduction, analogous to those with the geological strata (Figure 6a). One has to distinguish between

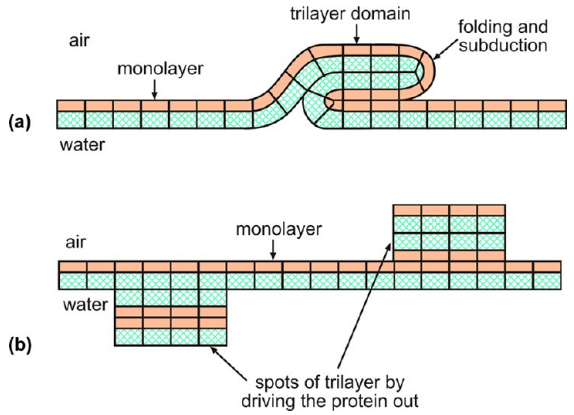

Figure 6. Sketch of two different mechanisms of trilayer formation in a hydrophobin monolayer subjected to compression: (a) Large trilayer domains can be formed from the monolayer by folding and subduction. (b) Numerous trilayer spots can appear by forcing protein molecules out of the monolayer, followed by spreading and self-assembly of the squeezed material into pimples of the adjacent bilayer. The spots may appear on both the upper (facing air) and lower (facing water) sides of the monolayer. The hydrophobic and hydrophilic parts of each HFBII molecules are shown with different colors.

folding and wrinkling (rippling) of protein layers. The present experiments indicate that the folding of a HFBII layer occurs during a process of continuous compression at a finite surface tension, $\sigma > 0$. As mentioned above, the theory[21] implies that periodic wrinkles may appear only in those portions of the elastic membrane, where locally $\sigma \approx 0$. (The Wilhelmy plate may register $\sigma > 0$, which refers to the tension in its close vicinity.) The leftmost parts (with the smallest slope) of the compression curves in Figure 1a can be explained with the

dx.doi.org/10.1021/la4005104 | Langmuir 2013, 29, 6053–6067

appearance of periodic wrinkles (E = 13.3 mN/m). In contrast, the long stage 6 for the upper curve in Figure 1a (E = 169.9 mN/m) could include folding and subduction (Figure 6a).

The trilayer protrusions in Figures 4 (panels a and c) and 5a could be formed by forcing protein molecules out of the compressed monolayer. The displaced molecules spread on the monolayer and form two additional layers (Figure 6b). The adhesive forces between the "hydrophilic" parts of the HFBII molecules, which are responsible for the formation of S-bilayer,[14] are playing a key role for the attachment of the squeezed protein to the monolayer. As sketched in Figure 6b, the squeezed material could be deposited on both the lower and upper side of the protein monolayer, but the present experiments do not allow us to distinguish between these two configurations.

4. DILATATIONAL ELASTICITY BY AREA OSCILLATIONS

In contrast with Surface Morphology Versus Surface Pressure, where the surface elasticity E was determined from the slope of the Π versus ln A dependence during compression at a fixed rate (Figure 1a), here we determine the elasticity by another method, viz., by experiments with oscillating surface area, A. The results for E obtained in the two different kinetic regimes are compared and discussed.

4.1. Oscillation Experiments and Data Interpretation.

These experiments have been carried out at different pH and concentrations of added NaCl to check the effect of the electrostatic interactions between the adsorbed HFBII molecules on the properties of the protein layer. As demonstrated below, the surface elasticity is not sensitive to the electrostatic interactions (an indication for predominant hydrophobic forces). However, the relaxation of the layer after a perturbation is faster at pH = 8.5, indicating a greater mobility of the charged HFBII molecules.

Figure 7a shows a typical set of experimental data obtained by the Langmuir trough. The variation of A has the shape of a triangular wave with the average area $\langle A\rangle$ = 94 cm^2 and amplitude $A_m \approx \pm$ 2.25 cm^2. The respective values of the surface pressure Π are also plotted versus time in Figure 7a. In general, the $\Pi(t)$ dependence is oscillatory with a decreasing mean value. There is no phase shift between the oscillations of $A(t)$ and $\Pi(t)$, which means that the effects of viscous dissipation are negligible, and the layer behaves as an almost ideal elastic body.

The surface elasticity is defined by eq 1. This equation can be integrated to give the instantaneous value of Π as a function of the area A, insofar as E remains approximately constant and equal to $\langle E\rangle$ within a sufficiently short time span:

$$\Pi(t) = \langle\Pi\rangle - \langle E\rangle \ln \frac{A(t)}{\langle A\rangle} \tag{2}$$

Equation 2 was used to fit the experimental data by means of a computer program written in Mathematica (Wolfram Research, Inc.). To achieve better precision and to avoid the superposition of electronic noise, we did not work with the obtained raw data for $A(t)$. Instead, the triangular-wave signal $A(t)$ was fitted with the respective Fourier series:[43]

$$A(t) = \langle A\rangle + A_m \frac{4}{\pi^2} \sum_{n=1,3,5,\ldots} \frac{1}{n^2} \cos\left(\frac{2\pi n}{T}(t - t_0)\right) \tag{3}$$

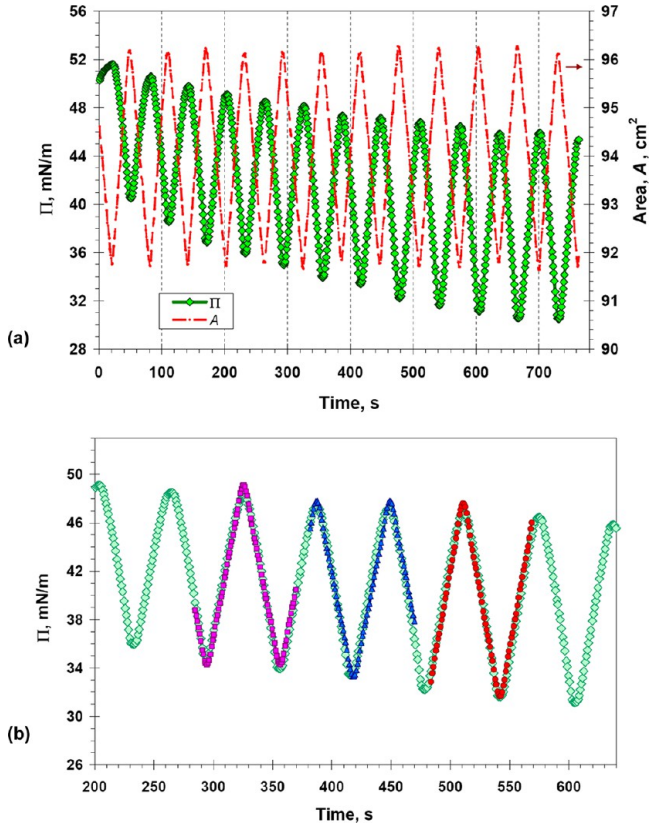

Figure 7. (a) Results for $\Pi(t)$ during oscillatory area deformation, performed after an initial continuous compression of the spread layer until Π reaches 50 mN/m; the water subphase has pH = 8.5 and contains 10 mM NaCl. (b) Fits of $\Pi(t)$ during three time intervals of duration 1.38T, shown with darker symbols; the period is T = 61.6 s, and the oscillatory curve is that from Figure 7a. The fits are made by eqs 2 and 3, where $\langle\Pi\rangle$ and $\langle E\rangle$ are determined as adjustable parameters.

where A_m is the amplitude, T is the period, and t_0 is a time shift. The measured $\Pi(t)$ was fitted with eq 2, with $A(t)$ from eq 3. $\langle\Pi\rangle$ and $\langle E\rangle$ were obtained from the fit as adjustable parameters. This procedure is carried out for groups of fixed number consecutive experimental points, which corresponds to a time interval on the order of the period T (but not necessarily equal to T). Figure 7b provides an illustration of how several pieces of the $\Pi(t)$ curve are fitted. The agreement with eq 2 is excellent. The determined $\langle\Pi\rangle$ and $\langle E\rangle$ values are assigned to the end points of the respective intervals, viz., t = 370, 470, and 569 s.

Furthermore, the group of experimental points selected for the fit is moved forward, by one-point steps, through the whole set of available data for a given oscillatory experiment, like that in Figure 7a. This method is a realization of sliding Fourier analysis. In such a manner, we determined the time dependences of the instantaneous average $\langle E\rangle$. Illustrative curves are plotted in Figure 8, where the different vertical axis for curve 3 is used because otherwise it overlaps with curve 2. Our purpose is to visualize the tendency of $\langle E\rangle$ to level off (to relax) at longer times.

The results in Figures 7 and 8 demonstrate that the layer undergoes gradual changes in the course of the cyclic expansion−compression. The mean surface pressure $\langle\Pi\rangle$ decreases, whereas the elastic modulus $\langle E\rangle$ increases. The evolution of these physical parameters can be attributed to the

dx.doi.org/10.1021/la4005104 | Langmuir 2013, 29, 6053−6067

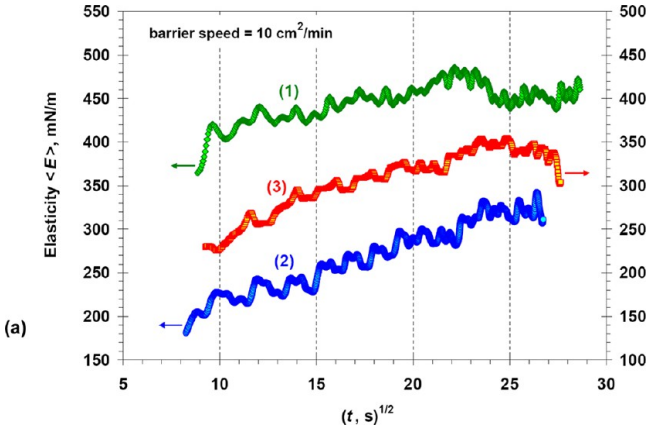

Figure 8. Plots of the averaged elasticity $\langle E \rangle$ vs the square root of time, $t^{1/2}$, calculated by means of eqs 2 and 3, using siding Fourier analysis (Figure 7). The experimental runs are as follows: (1) natural pH, preceding steps of oscillations and compression; (2) 10 mM NaCl, natural pH, preceding steps of oscillations and compression; (3) 10 mM NaCl, pH = 8.5, after continuous compression of the spread layer.

compaction of the HFBII interfacial layer. Indeed, as seen in Figures 2–5, the protein layer is not uniform but consists mostly of the monolayer and trilayer, with separate voids and thicker domains. Moreover, Figure 5 demonstrates that the thicker domains (pimples) aggregate in clusters upon area oscillations. In general, the compaction of the interfacial layer is related to the increase of its average thickness and mechanical rigidity, which is manifested by the rise of $\langle E \rangle$ in Figure 8. In addition, the formation of domains with three and more layers at a fixed number of HFBII molecules leads to shrinkage of the protein film in the lateral direction (i.e., to a decrease in the degree of its lateral compression that, in turns, leads to a decrease of the mean Π; see Figure 7).

It should also be noted that $\langle \Pi \rangle$ decreases linearly with $t^{1/2}$. Such a dependence indicates a diffusion mechanism of mass transport.[44,45] Because the adsorption of HFBII is irreversible (see Figure 1b and the related text), the aforementioned dependence cannot be related to adsorption–desorption of HFBII molecules. Consequently, following ref 20, we have to conclude that the redistribution of the protein between the interfacial domains and aggregates occurs under diffusion control. In other words, we are dealing with two-dimensional (2D) (surface) diffusion. This issue is further investigated in Model and Its Comparison with the Experiment. It should be also noted that the slopes of the $\langle \Pi \rangle$ versus $t^{1/2}$ lines increase at a higher pH but decrease at higher NaCl concentrations. This is an indication that the surface mobility of the protein molecules and aggregates increase when the electrostatic interactions are stronger.

4.2. Comparison of Data for Elasticity Measured in Different Kinetic Regimes. As mentioned above, the discontinuities in the lower experimental curve in Figure 1 correspond to area oscillations of a duration 12–13 min each. Figure 9a shows plots of a part of the obtained data as Π versus A. (All data are compared in Figure 9b.) Runs 1a, 2a, ..., 6a, in Figure 9 (panels a and b) correspond to the oscillatory experiments after the compression stages 1, 2, ..., 6 in Figure 1.

In Figure 9a, for each experimental dependence, the darker and brighter points correspond to expansion and compression, respectively. The points obtained in the two regimes almost coincide. This coincidence indicates that the viscous dissipation

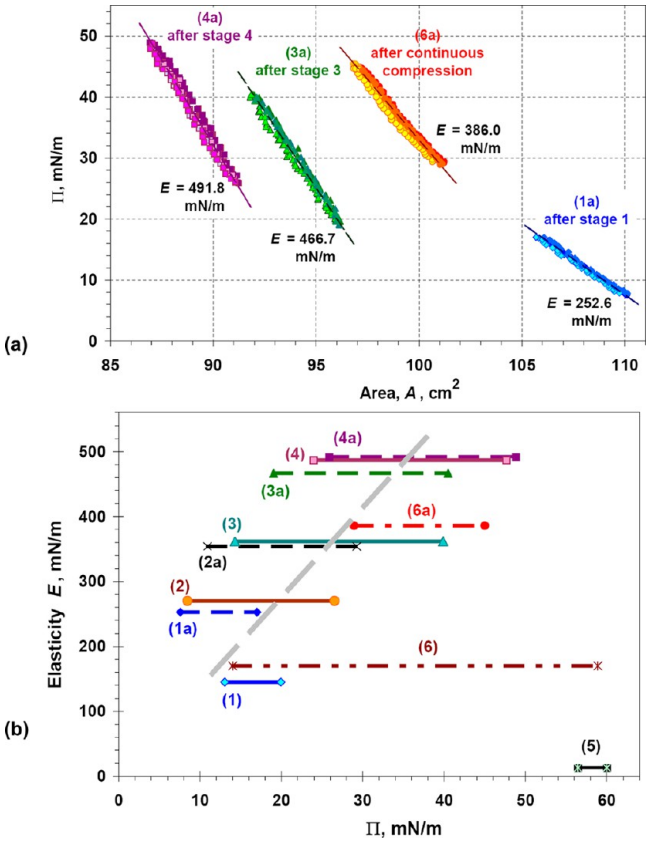

Figure 9. (a) Plots of Π vs A. Runs 1a, 3a, 4a, and 6a correspond to the oscillatory experiments after the compression stages of 1, 2, 4, and 6 in Figure 1. The darker and brighter points correspond to expansion and compression, respectively. (b) Plots of the dilatational elasticity E vs the surface pressure Π: Comparison of the E values from the compression stages 1, 2, ..., 6 in Figure 1, with those obtained in the oscillatory regime, 1a, 2a, ..., 6a, after the respective compression stage (Figure 9a). The range of variation of Π in each separate run is visualized.

effects are negligible, and the layer behaves as an elastic body. Note that the presence of viscous dissipation would lead to an ellipse-shaped dependence (i.e., a Lissajous plot).[23,46] In the limiting case of no viscous effects, the ellipse collapses into a segment, as in Figure 9a.

The slopes of the segments in Figure 9a give the respective values of the dilatational elasticity, E, which are also given in the figure. Oscillatory periods of 2–3 are taken at the long times, $t > 625$ s ($t^{1/2} > 25$ s$^{1/2}$) in Figure 8, where E levels off. Thus, the values of E estimated in Figure 9a (plotted also in Figure 9b) can be considered as relaxed values of the surface elasticity. The range of variation of Π for each plot in Figure 9a corresponds to the horizontal span of Π values in Figure 9b for the respective run.

In Figure 9b, we compare E values obtained from the $\Pi(A)$ data for the compression stages 1, 2, ..., 6 in Figure 1, with the E values obtained in the oscillatory regime, 1a, 2a, ..., 6a, after the respective compression stage. The elasticity E is plotted versus Π to visualize the range of variation of Π in the respective run. One sees that the oscillations lead to a considerable increase of E: compare runs 1 and 1a, runs 2 and 2a, and runs 3 and 3a. This behavior can be explained with a significant compaction of the protein layer during the oscillations, as seen also from Figures 5 and 8. (The continuous compression in Figure 1 was

dx.doi.org/10.1021/la4005104 | Langmuir 2013, 29, 6053–6067

carried out at a velocity of 10 cm^2/min, whereas the average velocity during oscillations was 4.5 cm^2/min; Figure 7a.) Runs 3a, 4, and 4a correspond to close values of E, which means that eventually the compaction reaches saturation. The saturation corresponds to an interfacial pattern like that in Figure 5a, which has been obtained by oscillations starting at Π = 50 mN/m.

The inclined dashed line in Figure 9b marks the overall tendency of E to increase with Π (i.e., with the layer's compaction for runs from 1 to 4a). The slope of this line, which is a dimensionless quantity, is 13.8 for HFBII. This slope is considerably greater than that measured with other proteins. For example, the respective slope is 6.1 for β-lactoglobulin at the air–water interface.[47] Also, the absolute value of E for HFBII, which can reach ≈500 mN/m (Figure 9b), is significantly greater than that for other proteins.[20,47,48] In view of the AFM images presented in Surface Morphology Versus Surface Pressure, the higher E values for hydrophobin can be explained with the ability of this protein to form compact and elastic interfacial layers, which are thicker than the monolayer (in average, a trilayer) at the air–water boundary.

In Figure 9b, runs 5, 6, and 6a represent deviations from the average tendency of E to increase almost linearly with Π, visualized by the inclined dashed line. As already mentioned, run 5 corresponds to the final stage of compression, at which periodic wrinkles appear. The small apparent value of E for run 5 is due to the fact that the interfacial layer undergoes wrinkling, rather than compression. For more details see the discussion on wrinkling after eq 1, as well as refs 19 and 21.

What concerns runs 6 and 6a, they represent the continuous compression in Figure 1, and the oscillation stage just after stopping the same compression at Π = 50 mN/m. The relatively low value of E for run 6 (Figure 9b) can be explained with processes of folding and subduction (Figure 6a), which can be accompanied by forcing the protein molecules out of the monolayer and the formation of pimples (Figure 6b). The oscillations help for the consolidation of the thicker domains that result in a considerable rise of elasticity; compare the values of E for runs 6 and 6a in Figure 9b.

Finally, it should be noted that most of the data in Figure 9b refer to Π > 22 mN/m, where the interfacial layers have solidified and the values of E are relatively high. In a previous study,[20] fluid hydrophobin layers (at Π < 22 mN/m) have been deliberately used, for which the values of E are lower. The reason is that the used method[20] has been the drop-shape analysis (DSA), which is based on fitting of the drop (or bubble) profile by the Laplace equation of capillarity. The Laplace equation is applicable only to interfaces with isotropic surface tension (i.e., fluid interfaces).

5. RELAXATION KINETICS AFTER EXPANSION OR COMPRESSION

In the previous sections, we investigated the rheological response of the system in regimes of continuous compression (Surface Morphology Versus Surface Pressure) and area oscillations (Dilatational Elasticity by Area Oscillations). In contrast, here we are dealing with another kinetic regime: a fast disturbance (interfacial expansion or compression) followed by a relaxation at a fixed area (A) for a period of ≥40 min. The data interpretation by a theoretical model gives information about the molecular mechanisms responsible for the observed relaxation processes.

5.1. Data for the Relaxation of Surface Pressure Π.

Figure 10a shows the time dependence of Π during a typical relaxation experiment. A spread HFBII layer was initially compressed from 150 to 90 cm^2 at a speed of 5 cm^2/min, which led to a relatively high surface pressure, Π = 65 mN/m. After that, the layer was left to relax for three hours. Next, the layer was quickly expanded to A = 100 cm^2, which was accompanied with a drop of Π down to 5 mN/m. Then, the layer was left again to relax for 40 min, which went along with a gradual increase of Π. Furthermore, additional compression–relaxation and expansion–relaxation cycles were carried out with the same protein layer. The vertical portions of the experimental curve

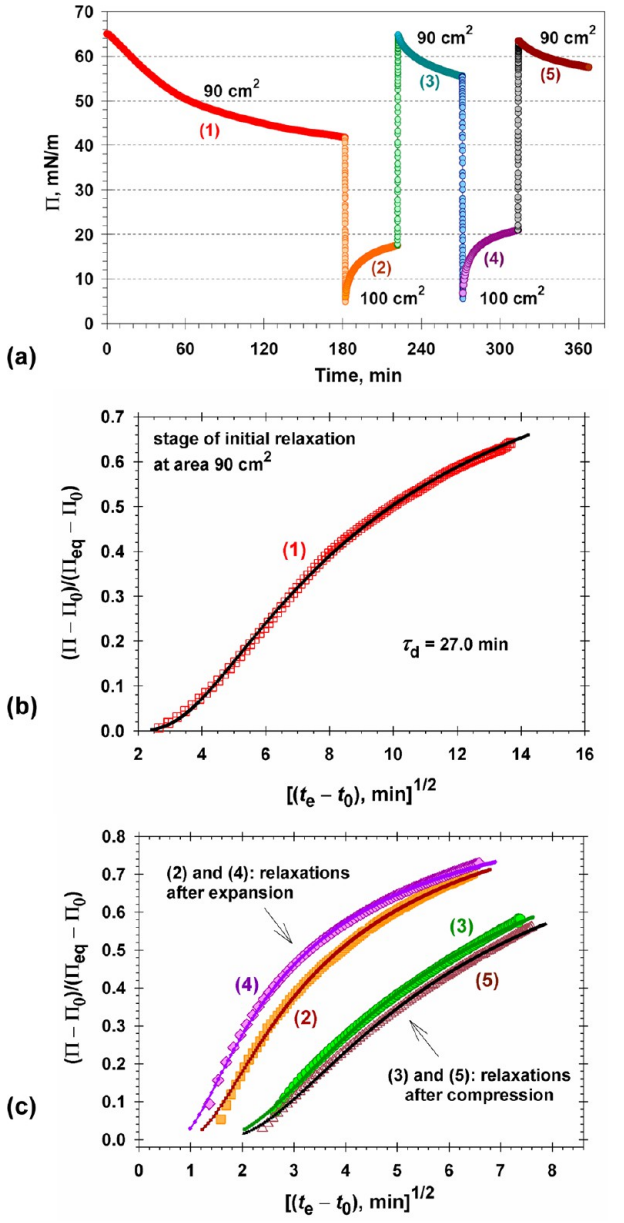

Figure 10. (a) Plot of data for the surface pressure Π vs time (t_e) for a spread HFBII layer that has been initially compressed from 150 to 90 cm^2 at a speed 5 cm^2/min, then left to relax (1) and further subjected to consecutive expansion–relaxation (2,4) and compression–relaxation (3,5) cycles. Fits (b) of the data from the 180 min relaxation stage 1 and (c) from the 40 min relaxation stages 2–5, in accordance with eq 9.

dx.doi.org/10.1021/la4005104 | Langmuir 2013, 29, 6053–6067

(Figure 10a) correspond to compressions or expansions at a speed of 20 cm^2/min.

In general, the data in Figure 10a indicate that the layer relaxes faster after expansion, in comparison with the relaxation after compression. Our next goal is to quantify the relaxation process and to obtain information about its kinetic mechanism (e.g., diffusion, barrier or mixed control).

5.2. Model and Its Comparison with the Experiment. We established that the relaxation kinetics complies with a diffusion mechanism. Let us consider purely surface 2D diffusion:

$$\frac{\partial \Gamma}{\partial t} = D_s \frac{\partial^2 \Gamma}{\partial x^2} \tag{4}$$

$\Gamma(x,t)$ is the surface density (adsorption) of mobile protein aggregates; D_s is their coefficient of surface diffusion, and the x axis is perpendicular to the barriers in the Langmuir trough. In general, the protein aggregates are polydispersed. Here, Γ and D_s represent average values. After an expansion, aggregates are released from the peripheries of consolidated protein domains and migrated by diffusion to cover the newly created interface. Conversely, after a compression, protein aggregates "condense" at the peripheries of the consolidated domains and are incorporated into them.[20] Thus, eq 4 effectively describes the motion of the protein molecules in the interfacial (multi)layer projected on the horizontal xy coordinate plane.

In the case of diffusion control, the surface concentration of protein aggregates near the periphery of a consolidated domain is equal to the equilibrium one:

$$\Gamma(x = 0, t) = \Gamma_{eq} \tag{5}$$

Just after the disturbance (a sudden expansion or compression) the surface concentration is

$$\Gamma(x > 0, t = 0) = \Gamma_0 \tag{6}$$

Because the diffusion is relatively slow, far from the consolidated domain we have

$$\Gamma(x \to \infty, t) = \Gamma_0 \tag{7}$$

Equations 4−7 represent a boundary problem, which can be solved by using the Laplace transform. The result reads

$$\frac{\Gamma(x, t) - \Gamma_0}{\Gamma_{eq} - \Gamma_0} = \mathrm{erfc}\left(\frac{x}{2\sqrt{D_s t}}\right) \tag{8}$$

with $\mathrm{erfc}(x)$ being the complementary error function. Further, we assume linear dependence between the variations of surface pressure and adsorption, $\Delta\Pi$ and $\Delta\Gamma$, which is fulfilled for small deformations and/or elastic behavior of the layer. Then, eq 8 can be represented in the form

$$\frac{\Pi(t) - \Pi_0}{\Pi_{eq} - \Pi_0} = \mathrm{erfc}\left(\sqrt{\frac{\tau_d}{t}}\right) \tag{9}$$

where $\tau_d = L^2/(4D_s)$ is a characteristic time of surface diffusion and L is a characteristic distance between two consolidated protein domains at the air−water interface; $\Pi_0 = \Pi(t = 0)$ and $\Pi_{eq} = \Pi(t \to \infty)$.

Equation 9 is similar (but not identical) to the known Sutherland formula.[44,49] The mathematical difference is that the Sutherland formula contains an additional multiplier $\exp(t/\tau_d)$, and t is in the numerator, viz., $\mathrm{erfc}[(t/\tau_d)^{1/2}]$. The physical difference is that the Sutherland formula refers to diffusion exchange of molecules between the interface and the adjacent bulk phase, whereas eq 9 describes a purely interfacial (two-dimensional) diffusion process.

To compare eq 9 with the experimental data for Π versus t_e, we have to adjust the zero of the time axis at the beginning of the considered relaxation process:

$$t = t_e - t_0 \tag{10}$$

Here, t_e is the experimentally recorded time in Figure 10a, whereas t_0 corresponds to the beginning of the respective relaxation process. For Π_0, we took the first experimental value of the surface pressure for the investigated relaxation stage.

Each of the five relaxation stages in Figure 10a was fitted with eq 9, along with eq 10, using τ_d, Π_{eq}, and t_0 as adjustable parameters. Figure 10b shows the fit of the longest, 180 min relaxation stage 1 in Figure 10a, whereas Figure 10c shows the fits of the shorter, 40 min relaxation stages 2−5. The values of the characteristic diffusion time, τ_d, obtained from these fits are given in Table 1.

Table 1. Characteristic Diffusion Time (τ_d) Obtained from the Fits of Data in Figure 10 (Panels b and c) by Eq 9

type of relaxation	run	τ_d (min)
after compression	(1)	27.0
after compression	(3)	10.5
after compression	(5)	12.2
after expansion	(2)	3.7
after expansion	(4)	2.3

In general, the data in Figure 10 (panels b and c) are in excellent agreement with eq 9. The relative variation $(\Pi - \Pi_0)/\Pi_0$ is considerable, especially for runs 2 and 4 (Figure 10a), which implies that the linear connection between $\Delta\Pi$ and $\Delta\Gamma$ is more likely due to the predominantly elastic behavior of the layer, rather than to small deformations. The data for τ_d in Table 1 show that the relaxation after expansion is considerably faster than after compression. In the former case, $\Pi_0 \approx 5$ mN/m, the layer is fluid, whereas in the latter case, $\Pi_0 \approx 65$ mN/m, the layer has certainly solidified; see Figure 10a and ref 20.

In the case of relaxation after expansion, the diffusing aggregates are expected to be smaller and the surrounding layer is fluid, which can explain the faster diffusion and the smaller τ_d. Conversely, in the case of relaxation after compression, the layer behaves as an elastic solid. In this case, one could hypothesize that fragments of thicker film can migrate by diffusion and merge into consolidated domains (clusters); see the pimples in Figures 4 and 5. Such a process could explain the greater τ_d in Table 1 for relaxation after compression.

6. CONCLUSIONS

The interfacial layers of hydrophobin possess the highest surface dilatational and shear elastic moduli among all investigated proteins.[1,3,20,23] In the present study, we combined Langmuir trough and AFM experiments to investigate the reasons for the special properties of HFBII layers spread on the air−water interface. The experimental data and their analysis lead to the following physical picture of the changes that occur in hydrophobin interfacial layers subjected to deformations.

Having once attached to the air−water interfaces, the hydrophobin remains there [i.e., there is no desorption (Figure 1b)]. The ellipsometric measurements with spread monolayers give an average thickness, which is greater than that of a

dx.doi.org/10.1021/la4005104 | Langmuir 2013, 29, 6053−6067

monolayer (Figure 1c). The AFM measurements show the mesoscopic structure of the spread layers, which are rather inhomogeneous: voids, monolayer, and multilayer domains are observed (Figure 2). A continuous compression of the layer leads to filling the voids and to transformation of a part of the monolayer into trilayer. The AFM images indicate that two different patterns of trilayer are formed. The trilayer can appear in the form of large surface domains (Figure 3b), which could be explained with a folding and subduction (Figure 6a). In addition, the trilayer can appear in the form of numerous protrusions (pimples) of submicrometer diameter [Figures 4 (panels a and c) and 5a], which can be produced by forcing HFBII molecules out of the monolayer and their self-assembly into adjacent bilayers (Figure 6b). The formation of such type of structures is related to the fact that not only the hydrophobic but also the hydrophilic parts of the HFBII molecules can adhere to each other in the water medium.[14] Coexistence between monolayer and trilayer has been observed also in the spread layers of some phospholipids.[42]

If a hydrophobin layer is subjected to oscillations in the Langmuir trough, its elasticity E considerably increases and can reach 400−500 mN/m (Figures 8 and 9). This can be explained with a compaction of the protein layer. The compaction is related to a decrease in the area fraction of the voids and an increase in the area fractions of trilayers and multilayers. In addition, some fragmentary domains merge with each other to form a consolidated elastic film.

Despite the complex structure of the hydrophobin layers, the relaxation of their tension after expansion or compression follows the same relatively simple law [Figure 10 (panels b and c)], given by eq 9, which refers to the surface diffusion of protein aggregates within the interfacial layer. This result implies that the relaxation probably occurs through splitting or merging of HFBII aggregates, which are transported by surface diffusion. The characteristic diffusion time after compression is longer than after expansion (Table 1), which can be explained with the impeding of diffusion in the more compact interfacial layer.

The present article sheds light on the relation between the mesoscopic structure and the unique mechanical properties of hydrophobin interfacial layers that find applications for the production of foams and emulsions of extraordinary stability,[1−8] for the immobilization of functional molecules at surfaces,[50−52] and as coating agents for surface modification.[53−55]

AUTHOR INFORMATION

Corresponding Author

*E-mail: pk@lcpe.uni-sofia.bg. Tel: (+359) 2-8161262. Fax: (+359) 2-9625643.

Notes

The authors declare no competing financial interest.

ACKNOWLEDGMENTS

The authors gratefully acknowledge the support from Unilever Research, from the National Science Fund of Bulgaria, Grant DO-02-121/2009, from the FP7 project Beyond-Everest, and from COST Action CM1101. The authors thank Prof. Krassimir D. Danov for the helpful discussions and Prof. Stoyan Russev and Dr. Gichka Tsutsumanova for their help in the ellipsometric measurements.

REFERENCES

(1) Cox, A. R.; Cagnol, F.; Russell, A. B.; Izzard, M. J. Surface properties of class II hydrophobins from *Trichoderma reesei* and influence on bubble stability. *Langmuir* **2007**, *23*, 7995−8002.

(2) Cox, A. R.; Aldred, D. L.; Russell, A. B. Exceptional stability of food foams using class II hydrophobin HFBII. *Food Hydrocolloids* **2009**, *23*, 366−376.

(3) Blijdenstein, T. B. J.; de Groot, P. W. N.; Stoyanov, S. D. On the link between foam coarsening and surface rheology: Why hydrophobins are so different. *Soft Matter* **2010**, *6*, 1799−1808.

(4) Blijdenstein, T. B. J.; Ganzevles, R. A.; de Groot, P. W. N.; Stoyanov, S. D. On the link between surface rheology and foam disproportionation in mixed hydrophobin HFBII and whey protein systems. *Colloids Surf., A* **2013**, DOI: 10.1016/j.colsurfa.2012.12.040.

(5) Burke, J.; Cox, A.; Petkov, J.; Murray, B. S. Interfacial rheology and stability of air bubbles stabilized by mixtures of hydrophobin and β-casein. *Food Hydrocolloids* **2013**, DOI: 10.1016/j.foodhyd.2012.11.026.

(6) Reger, M.; Sekine, T.; Okamoto, T.; Hoffmann, H. Unique emulsions based on biotechnically produced hydrophobins. *Soft Matter* **2011**, *7*, 8248−8257.

(7) Reger, M.; Sekine, T.; Okamoto, T.; Watanabe, K.; Hoffmann, H. Pickering emulsions stabilized by novel clay−hydrophobin synergism. *Soft Matter* **2011**, *7*, 11021−11030.

(8) Reger, M.; Sekine, T.; Hoffmann, H. Boosting the stability of protein emulsions by the synergistic use of proteins and clays. *Colloid Polym. Sci.* **2012**, *290*, 631−640.

(9) Cox, P. W.; Hooley, P. Hydrophobins: New prospects for biotechnology. *Fungal Biology Reviews* **2009**, *23*, 40−47.

(10) Wessels, J. G. H. Hydrophobins, unique fungal proteins. *Mycologist* **2000**, *14*, 153−159.

(11) Tchuenbou-Magaia, F. L.; Norton, I. T.; Cox, P. W. Hydrophobins stabilised air-filled emulsions for the food industry. *Food Hydrocolloids* **2009**, *23*, 1877−1885.

(12) Khalesi, M.; Deckers, S. M.; Gebruers, K.; Vissers, L.; Verachtert, H.; Derdelinckx, G. Hydrophobins: Exceptional proteins for many applications in brewery environment and other bioindustries. *Cerevisia* **2012**, *37*, 3−9.

(13) Hakanpää, J.; Paananen, A.; Askolin, S.; Nakari-Setälä, T.; Parkkinen, T.; Penttilä, M.; Linder, M. B.; Rouvinen, J. Atomic resolution structure of the HFBII hydrophobin, a self-assembling amphiphile. *J. Biol. Chem.* **2004**, *279*, 534−539.

(14) Basheva, E. S.; Kralchevsky, P. A.; Danov, K. D.; Stoyanov, S. D.; Blijdenstein, T. B. J.; Pelan, E. G.; Lips, A. Self-assembled bilayers from the protein HFBII hydrophobin: Nature of the adhesion energy. *Langmuir* **2011**, *27*, 4481−4488.

(15) Kisko, K.; Szilvay, G. R.; Vuorimaa, E.; Lemmetyinen, H.; Linder, M. B.; Torkkeli, M.; Serimaa, R. Self-assembled films of hydrophobin proteins HFBI and HFBII studied in situ at the air/water interface. *Langmuir* **2009**, *25*, 1612−1619.

(16) Linder, M. B. Hydrophobins: Proteins that self assemble at interfaces. *Curr. Opin. Colloid Interface Sci.* **2009**, *14*, 356−363.

(17) Szilvay, G. R.; Paananen, A.; Laurikainen, K.; Vuorimaa, E.; Lemmetyinen, H.; Peltonen, J.; Linder, M. B. Self-assembled hydrophobin protein films at the air−water interface: Structural analysis and molecular engineering. *Biochemistry* **2007**, *46*, 2345−2354.

(18) Paananen, A.; Vuorimaa, E.; Torkkeli, M.; Penttilä, M.; Kauranen, M.; Ikkala, O.; Lemmetyinen, H.; Serimaa, R.; Linder, M. B. Structural hierarchy in molecular films of two class II hydrophobins. *Biochemistry* **2003**, *42*, 5253−5258.

(19) Basheva, E. S.; Kralchevsky, P. A.; Christov, N. C.; Danov, K. D.; Stoyanov, S. D.; Blijdenstein, T. B. J.; Kim, H.-J.; Pelan, E. G.; Lips, A. Unique properties of bubbles and foam films stabilized by HFBII Hydrophobin. *Langmuir* **2011**, *27*, 2382−2392.

(20) Alexandrov, N. A.; Marinova, K. G.; Gurkov, T. D.; Danov, K. D.; Kralchevsky, P. A.; Stoyanov, S. D.; Blijdenstein, T. B. J.; Arnaudov, L. N.; Pelan, E. G.; Lips, A. Interfacial layers from the protein HFBII hydrophobin: Dynamic surface tension, dilatational

elasticity and relaxation times. *J. Colloid Interface Sci.* **2012**, *376*, 296−306.
(21) Danov, K. D.; Kralchevsky, P. A.; Stoyanov, S. D. Elastic Langmuir layers and membranes subjected to unidirectional compression: Wrinkling and collapse. *Langmuir* **2010**, *26*, 143−155.
(22) Radulova, G. M.; Golemanov, K.; Danov, K. D.; Kralchevsky, P. A.; Stoyanov, S. D.; Arnaudov, L. N.; Blijdenstein, T. B. J.; Pelan, E. G.; Lips, A. Surface shear rheology of adsorption layers from the protein HFBII hydrophobin: effect of added β-casein. *Langmuir* **2012**, *28*, 4168−4177.
(23) Danov, K. D.; Radulova, G. M.; Kralchevsky, P. A.; Golemanov, K.; Stoyanov, S. D. Surface shear rheology of hydrophobin adsorption layers: Laws of viscoelastic behaviour with applications to long-term foam stability. *Faraday Discuss.* **2012**, *158*, 195−221.
(24) Panaiotov, I.; Dimitrov, D. S.; Ter-Minassian-Saraga, L. Dynamics of insoluble monolayers. II. Viscoelastic behavior and Marangoni effect for mixed protein phospholipid films. *J. Colloid Interface Sci.* **1979**, *72*, 49−53.
(25) Panaiotov, I.; Ivanova, Tz.; Proust, J.; Boury, F.; Denizot, B.; Keough, K.; Taneva, S. Effect of hydrophobic protein SP-C on structure and dilatational properties of the model monolayers of pulmonary surfactant. *Colloids Surf., B* **1996**, *6*, 243−260.
(26) Wierenga, P. A.; Meinders, M. B. J.; Egmond, M. R.; Voragen, A. G. J.; de Jongh, H. H. J. Quantitative description of the relation between protein net charge and protein adsorption to air−water interfaces. *J. Phys. Chem., B* **2005**, *109*, 16946−16952.
(27) Balashev, K.; Ivanova, Tz.; Mircheva, K.; Panaiotov, I. Savinase proteolysis of insulin Langmuir monolayers studied by surface pressure and surface potential measurements accompanied by atomic force microscopy (AFM) imaging. *J. Colloid Interface Sci.* **2011**, *360*, 654−661.
(28) Petkov, J. T.; Gurkov, T. D.; Campbell, B. E.; Borwankar, R. P. Dilatational and shear elasticity of gel-like protein layers on air/water interface. *Langmuir* **2000**, *16*, 3703−3711.
(29) Houmadi, S.; Rodriguez, R. D.; Longobardi, S.; Giardina, P.; Fauré, M. C.; Giocondo, M.; Lacaze, E. Self-assembly of Hydrophobin protein rodlets studied with atomic force spectroscopy in dynamic mode. *Langmuir* **2012**, *28*, 2551−2557.
(30) Askolin, S.; Linder, M.; Scholtmeijer, K.; Tenkanen, M.; Penttila, M.; de Vocht, M. L.; Wosten, H. A. B. Interaction and comparison of a class I hydrophobin from Schizophyllum commune and class II hydrophobins from Trichoderma reesei. *Biomacromolecules* **2006**, *7*, 1295−1301.
(31) Russev, S. C.; Arguirov, Tz. V. Rotating analyzer: Fixed analyzer ellipsometer based on null type ellipsometer. *Rev. Sci. Instrum.* **1999**, *70*, 3077−3082.
(32) Gurkov, T. D.; Russev, S. C.; Danov, K. D.; Ivanov, I. B.; Campbell, B. Monolayers of globular proteins on the air/water interface: Applicability of the Volmer equation of state. *Langmuir* **2003**, *19*, 7362−7369.
(33) Helfrich, W.; Servuss, R.-M. Undulations, steric interaction and cohesion of fluid membranes. *Nuovo Cimento* **1984**, *D3*, 137−151.
(34) Evans, E. Equilibrium "wetting" of surfaces by membrane-covered vesicles. *Adv. Colloid Interface Sci.* **1992**, *39*, 103−128.
(35) Mallouri, R.; Keramidas, A. D.; Brezesinski, G.; Leontidis, E. Monolayer properties of surface-active metalorganic complexes with a tunable headgroup. *J. Colloid Interface Sci.* **2008**, *317*, 544−555.
(36) Steffens, S.; Oldendorf, J.; Haufe, G.; Galla, H.-J. Organized collapse structures in mixtures of chiral ethyl 2-azido-4-fluoro-3-hydroxystearates. *Langmuir* **2006**, *22*, 1428−1435.
(37) Kundu, S.; Datta, A.; Hazra, S. Effect of metal ions on monolayer collapses. *Langmuir* **2005**, *21*, 5894−5900.
(38) Zhang, Y.; Fischer, T. M. Fold-speed control in collapsing mixed phospholipid monolayers. *J. Phys. Chem. B* **2005**, *109*, 3442−3445.
(39) Gavranovic, G. T.; Kurtz, R. E.; Golemanov, K.; Lange, A.; Fuller, G. G. Interfacial rheology and structure of straight-chain and branched hexadecanol mixtures. *Ind. Eng. Chem. Res.* **2006**, *45*, 6880−6884.
(40) Milner, S. T.; Joanny, J.-F.; Pincus, P. Buckling of Langmuir monolayers. *Europhys. Lett.* **1989**, *9*, 495−500.
(41) Zhang, X. L.; Penfold, J.; Thomas, R. K.; Tucker, I. M.; Petkov, J. T.; Bent, J.; Cox, A.; Campbell, R. A. Adsorption behavior of hydrophobin and hydrophobin/surfactant mixtures at the air-water interface. *Langmuir* **2011**, *27*, 11316−11323.
(42) Saccani, J.; Castano, S.; Beaurain, F.; Laguerre, M.; Desbat, B. Stabilization of phospholipid multilayers at the air−water interface by compression beyond the collapse: A BAM, PM-IRRAS, and molecular dynamics study. *Langmuir* **2004**, *20*, 9190−9197.
(43) Arfken, G. *Mathematical Methods for Physicists*; Academic Press: New York, 1970.
(44) Joos, P. *Dynamic Surface Phenomena*. VSP: Utrecht, The Netherlands, 1999.
(45) Eastoe, J.; Dalton, J. S. Dynamic surface tension and adsorption mechanisms of surfactants at the air-water interface. *Adv. Colloid Interface Sci.* **2000**, *85*, 103−144.
(46) Hyun, K.; Wilhelm, M.; Klein, C. O.; Cho, K. S.; Nam, J. G.; Ahn, K. H.; Lee, S. J.; Ewoldt, R. H.; McKinley, G. H. A review of nonlinear oscillatory shear tests: Analysis and application of large amplitude oscillatory shear (LAOS). *Prog. Polym. Sci.* **2011**, *36*, 1697−1753.
(47) Lucassen-Reynders, E. H.; Benjamins, J.; Fainerman, V. B. Dilational rheology of protein films adsorbed at fluid interfaces. *Curr. Opin. Colloid Interface Sci.* **2010**, *15*, 264−270.
(48) Benjamins, J.; Lyklema, J.; Lucassen-Reynders, E. H. Compression/expansion rheology of oil/water interfaces with adsorbed proteins. Comparison with the air/water surface. *Langmuir* **2006**, *22*, 6181−6188.
(49) Sutherland, K. L. The kinetics of adsorption at liquid surfaces. *Aust. J. Sci. Res.* **1952**, *5*, 683−696, , http://dx.doi.org/10.1071/CH9520683.
(50) Zhao, Z.-X.; Qiao, M.-Q.; Yin, F.; Shao, B.; Wu, B.-Y.; Wang, Y.-Y.; Wang, X.-S.; Qin, X.; Li, S.; Yu, L.; Chen, Q. Amperometric glucose biosensor based on self-assembly hydrophobin with high efficiency of enzyme utilization. *Biosens. Bioelectron.* **2007**, *22*, 3021−3027.
(51) Qin, M.; Wang, L.-K.; Feng, X.-Z.; Yang, Y.-L.; Wang, R.; Wang, C.; Yu, L.; Shao, B.; Qiao, M.-Q. Bioactive surface modification of mica and poly(dimethylsiloxane) with hydrophobins for protein immobilization. *Langmuir* **2007**, *23*, 4465−4471.
(52) Asakawa, K.; Tahara, S.; Nakamichi, M.; Takehara, K.; Ikeno, S.; Linder, M.; Haruyama, T. The amphiphilic protein HFBII as a genetically taggable molecular carrier for the formation of a self-organized functional protein layer on a solid surface. *Langmuir* **2009**, *25*, 8841−8844.
(53) Lumsdon, S. O.; Green, J.; Stieglitz, B. Adsorption of hydrophobin proteins at hydrophobic and hydrophilic interfaces. *Colloids Surf., B* **2005**, *44*, 172−178.
(54) Li, X.; Hou, S.; Feng, X.; Yu, Y.; Ma, J.; Li, L. Patterning of neural stem cells on poly(lactic-co-glycolic acid) film modified by hydrophobin. *Colloids Surf., B* **2009**, *74*, 370−374.
(55) Wang, Z.; Lienemann, M.; Linder, M. M. B. Mechanisms of protein adhesion on surface films of hydrophobin. *Langmuir* **2010**, *26*, 8491−8496.